Rock-physics analysis of clay-rich source rocks on the Norwegian Shelf

Per Avseth[1] and José M. Carcione[2]

Abstract

Rock-physics trends and properties of clay-rich source rocks are investigated in selected wells in the North Sea and Norwegian Sea. Properties can vary significantly because of burial compaction, composition, diagenesis, organic richness, and maturation. The many competing effects can be difficult to disentangle in traditional rock-physics crossplots. However, nearly all the source-rock data in the study are bounded nicely by linear trends that are based on rock-physics models, in acoustic-impedance (AI) versus shear-impedance (SI) crossplots. These reference models serve as a nice screening tool for organic richness and/or maturation level (i.e., hydrocarbon generation and expulsion), regardless of burial depth. The use of rock-physics templates for the early mature to mature stage of clay-rich source rocks is demonstrated by combining a simple basin-modeling approach with a rock-physics model using Backus average in which the organic-rich shale is represented by a transverse isotropic mixture of clays, kerogen, and hydrocarbons. The resulting templates are bounded nicely by reference trends and explain some of the observed trends in the data. However, the local presence of carbonaceous material and diagenesis within the source rock, which have not been accounted for in the rock-physics modeling, might explain why some of the data points have higher impedances and lower V_P/V_S than the template models. Finally, source rocks with hydrocarbon saturation can cause AVO signatures similar to hydrocarbon-filled sands and therefore represent false positives in exploration.

Introduction

By linking geologic processes and burial history of organic-rich shales with rock-physics properties, we can better predict the expected seismic signatures of organic-rich shales as a function of total organic carbon (TOC) and maturity. Moreover, mature source rocks might give seismic signatures similar to hydrocarbon-filled reservoirs, and a good geophysical understanding of organic-rich source rocks is also important to avoid false positives during exploration (Avseth et al., 2014).

Løseth et al. (2011) show that TOC content in source rocks can be quantified from acoustic impedance. Hu et al. (2015) map organic richness of the Eagle Ford Shale from inversion data of acoustic impedance and shear impedance combined, based on rock-physics models. Bandyopadhyay et al. (2012) demonstrate the ambiguities and uncertainties when characterizing organic-rich shales, and they also include V_P/V_S and anisotropy to better quantify TOC from rock-physics models. Qin et al. (2014) investigate the effect of maturation on the rock-physics properties of organic-rich shales.

In this study, we first do rock-physics screening of the Kimmeridge Shale equivalent in selected wells in the North Sea and Norwegian Sea. We compare well-log data with some useful reference trends in crossplots of acoustic impedance versus V_P/V_S and shear impedance. These reference models include an inorganic shale trend and an organic-rich shale trend. The inorganic shale trend represents conventional shale as defined by Vernik and Kachanov (2010) and was used by Khadeeva and Vernik (2014) as a reference trend. The organic-rich shale trend is based on the theory of Vernik and Milovac (2011) and was presented by Hu et al. (2015), representing a shale with 7.5% TOC.

Because this trend was calibrated originally to a mature, marly source rock of Eagle Ford, it also will reflect the presence of hydrocarbons inside the source rock. In this study, we will refer to this as the "hot-shale" reference trend, whereas we refer to the inorganic shale trend as the "wet-shale" reference trend. We expect neither of these trends to be directly applicable to our Norwegian Sea clay-rich source rocks, but they will serve as useful reference trends for source rocks with varying TOC and at different maturation stages.

In this study, we also compare our well-log data from the Norwegian Shelf with ultrasonic laboratory measurements conducted on cores from the Kimmeridge Shale in the North Sea (Vernik, 1995; Carcione et al., 2011). Then we investigate the data for various geologic trends, including the effects of TOC, composition, diagenesis, burial depth, and hydrocarbon generation (i.e., maturation). We use the rock-physics templates for clay-rich source rocks proposed by Carcione and Avseth (2015) to detect the degree of maturation from seismic properties. Carcione and Avseth (2015) propose a modeling methodology to build these templates for immature versus mature source rocks.

To model kerogen-oil and oil-gas conversions, we assumed a basin-evolution model with constant sedimentation rate, geothermal gradient, and first-order kinetic (Arrhenius) reaction. The bulk modulus of the oil-gas mixture is calculated by a mesoscopic-loss model, and the stiffnesses of the kerogen/fluid mixture are obtained with the Kuster and Toksöz model, assuming that the fluid is included in the kerogen matrix. Finally, we use Backus averaging to mix the organic matter with the shale, where thermal transformation of smectite to illite is taken into account. More details about the modeling are found in Carcione and Avseth (2015).

The Kimmeridge Shale equivalent is referred to as the Draupne Formation in the North Sea and the Spekk Formation in the Norwegian Sea. Unfortunately, very few wells with measured V_P and V_S have penetrated thick, massive sections of this organic-rich shale. This is because most wells have targeted structural highs, where this interval is either missing or condensed. Moreover, shear-wave information seldom is acquired in shaley intervals if these are not stratigraphically within or adjacent to target reservoir intervals.

Nevertheless, we have information from four vertical or near-vertical wells in the North Sea and two vertical wells in the Norwegian Sea, all of which have both P-wave and S-wave

[1]Tullow Oil.
[2]OGS.

DOI information... http://dx.doi.org/10.1190/tle34101xxx.1.

velocity information from the Kimmeridge Shale equivalent. Hence, we can estimate the V_P/V_S ratios for the organic-rich shales in these wells. In addition, we have density information that allows for estimation of acoustic impedance and shear impedance. The density also can be used to estimate TOC within the source-rock intervals, and we have TOC measurements from one well in the Norwegian Sea and one well in the North Sea for calibration. Comparing well-log data with the rock-physics templates allow us to interpret important trends in the data.

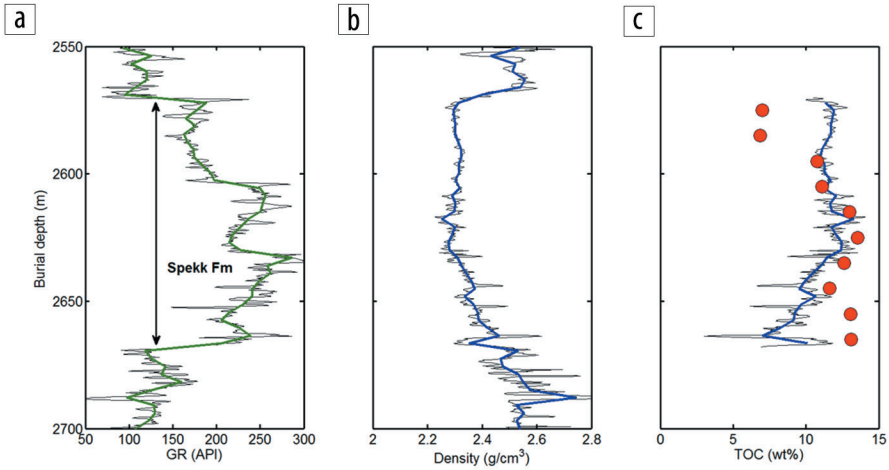

Figure 1. (a) and (b) Well-log data and (c) TOC measurements from well 6507/11-6, Norwegian Sea. The Spekk Formation is characterized by high gamma-ray values and relatively low densities. TOC content also is estimated from the density log within the Spekk interval and is calibrated with the measurements (red circles).

Rock-physics screening and burial-trend analysis

The first part of this study is devoted to rock-physics screening of selected wells from the Norwegian Sea and North Sea. We will compare well-log data from the Kimmeridge Shale equivalent on the Norwegian Shelf with the wet-shale and hot-shale reference trends based on Khadeeva and Vernik (2014) and Hu et al. (2015), respectively. Furthermore, we will try to explore for trends in the data and interpret those in terms of geologic parameters such as burial, composition, and maturation level. The Kimmeridge Shale is predominantly a marine source rock with type II kerogen (oil and gas prone).

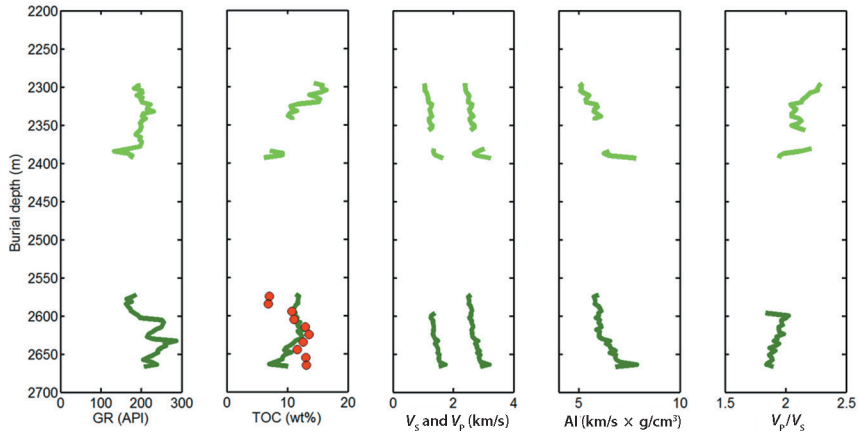

Figure 2. Data from two selected wells (upper: 6507/8-7; lower: 6507/11-6) in the Norwegian Sea, capturing the Spekk Formation organic-rich shale interval. The present-day burial is near maximum burial because there has been minimal uplift in the area, and both intervals are found to be immature.

Two wells from the Norwegian Sea are available for this study, in which we have both measured V_P and V_S in the Kimmeridge Shale interval, referred to as the Spekk Formation in this area. We also have TOC data from one of the wells, 6507/11-6. Hence, we can use the density log and estimate TOC using the TOC data for calibration. This can be done by using the empirical formula proposed by Vernik and Landis (1996):

$$\mathrm{TOC(wt\%)} = 67 \times \frac{\rho_k(\rho_s - \rho_b)}{\rho_b(\rho_s - \rho_k)} \qquad (1)$$

where ρ_k is the density of kerogen, which equals 1.3 g/cm^3, ρ_s is the density of the mixed shale (smectite and illite), and ρ_b is the measured bulk density. The density of the mixed shale will vary as a function of burial depth, and this parameter will be a fudge parameter during the calibration because exact mineralogical composition in the studied organic-rich shales is not known.

The Kimmeridge Shale is known to be rich in clay, and the clay mineralogy is dominated by smectite and illite, with mineral densities of 2.2 g/cm^3 and 2.9 g/cm^3, respectively (Carcione and Avseth, 2015). The shales tend to be rich in smectite down to temperatures of about 70°C (corresponding to a burial depth of about 2 km on the Norwegian Shelf), when smectite will transform to illite, with microcrystalline quartz as a by-product (Bjørlykke, 2015).

Figure 1 shows the results of the TOC calibration for well 6507/11-9. We need to use a shale density of 2.75 to obtain a relatively good match with the TOC data. This indicates that the shale matrix is probably rich in illite and richer in quartz at this depth.

Figure 2 shows well-log data from both the Norwegian Sea wells (6507/8-7 and 6507/11-6), including only data from the Spekk Formation interval. The data comprise gamma ray, TOC (estimated from density), and velocities (V_P and V_S). The TOC estimate for well 6507/8-7 is derived by using a slightly lower shale density (2.65 g/cm^3). We expect the shale to have slightly more smectite because the Spekk Formation is buried about 300 m shallower in this well. We also display the computed acoustic impedance and V_P/V_S, and all logs have been upscaled using a

blocking-average approach (20 log samples in each block = 20 × 15.24 cm) to avoid high-frequency scatter in the data.

The data in Figure 2 clearly show some depth trend from one well to the other. However, we also see significant variability within the Spekk Formation interval in both wells. Most of the Spekk interval in both wells has a TOC content that exceeds 10%.

Next, we compare these well-log data with the wet-shale and hot-shale reference trends introduced above, both in terms of acoustic impedance versus V_P/V_S and acoustic impedance versus shear impedance (SI) (Figure 3). We also superimpose the ultrasonic data measured normal to bedding on selected core samples from the Kimmeridge Shale in the North Sea (Vernik, 1995; also see Carcione et al., 2011).

We see that all the data in both the wells plot between the wet-shale and hot-shale reference trends. Note that because the Norwegian Sea organic-rich shales are very clay rich, they plot closer to the wet-shale reference trend even if they are organic rich. Furthermore, we observe that the ultrasonic measurements by Vernik (1995) plot nicely along the same trend as the well-log data from the Norwegian Sea.

The Spekk Formation in the deeper well, 6507/11-6, has hydrogen index (HI) values in the range or 200 to 300 (average 251), and the vitrinite reflectance is 0.48. This is close to the expected transition from immature to oil mature for marine source rocks with kerogen type II (Tissot and Welte, 1984). Hence, we do not expect hydrocarbons to have been generated inside the kerogen of the organic-rich shales in either of these wells.

Next, we analyze data from selected wells in the North Sea. Four wells are analyzed, and we refer to these as NS-1, NS-2, NS-3, and NS-4, with increasing burial depth for the organic-rich shales in the different wells. Figure 4 shows well-log data, including gamma ray and density, and TOC data from well NS-1. We also have estimated TOC using equation 1, and we obtain a good match when we use a shale density of 2.55 g/cm^3. This is slightly lower than what we used above. This makes sense because the Kimmeridge Shale equivalent, here called the Draupne Formation, is buried more shallowly than the two Norwegian Sea wells studied above. We expect smectite volume fraction to be higher.

Figure 5 shows the Draupne Formation in all the four North Sea wells plotted along with the same reference trends as for the Norwegian Sea wells (all data have been upscaled to avoid high-frequency scatter and to make them more nearly similar to seismic resolution). In NS-1, on the flank of the Horda Platform, the burial depth of the Draupne Shale is only about 1.7 km. The burial depth has likely been a few hundred meters deeper in the geologic past, but the depths and temperatures never have been high enough to make the source rock mature (HI values are mostly in the range of 450 to 500 and an average of 473, which are representative of an immature marine source rock, kerogen type II; see Glennie, 1998.)

Nevertheless, we see that a large fraction of the Draupne Shale plots along the hot-shale trend and not closer to the wet-shale trend, as we would expect for a clay-rich, organic-rich shale. This observation is a puzzle, and we will get back to what is causing this "anomalous" behavior later in this article.

In the next well, NS-2, only 6 km from NS-1 but buried slightly deeper (~ 1850 m), we observe that the Draupne Shale interval plots closer to the wet-shale trend. In well NS-3, the

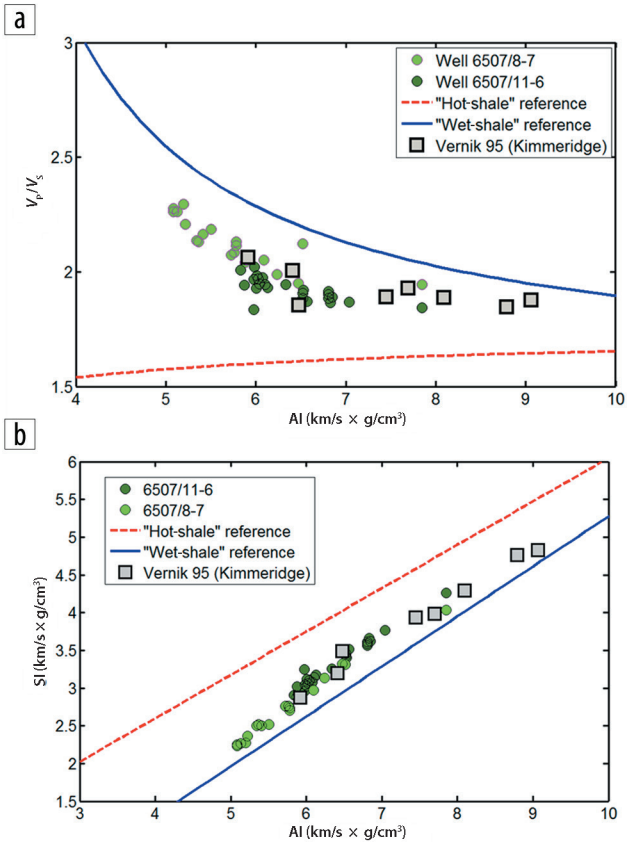

Figure 3. Crossplot analysis of well-log data from the Spekk Formation in the Norwegian Sea. The organic-rich shale is clay rich and immature in both these wells, and the data plot closer to the "wet-shale" reference trend.

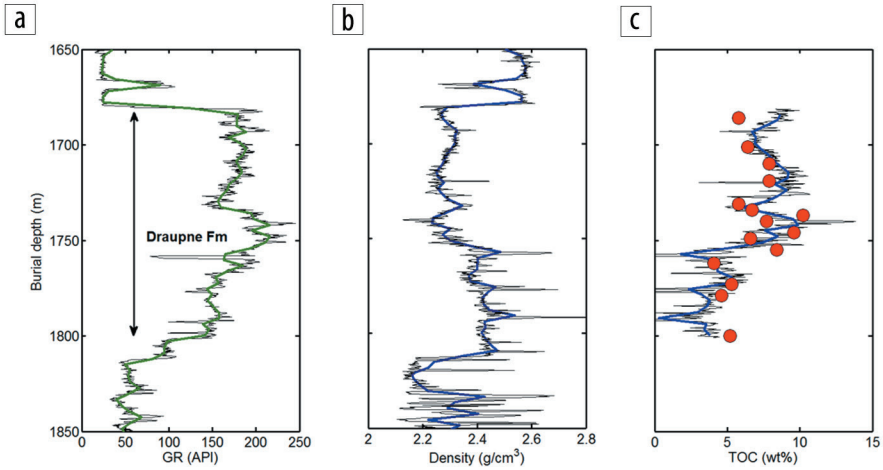

Figure 4. (a) Gamma ray, (b) density, and (c) TOC in well NS-1. The TOC data include predicted TOC log from density, and red circles are TOC measurements from core samples.

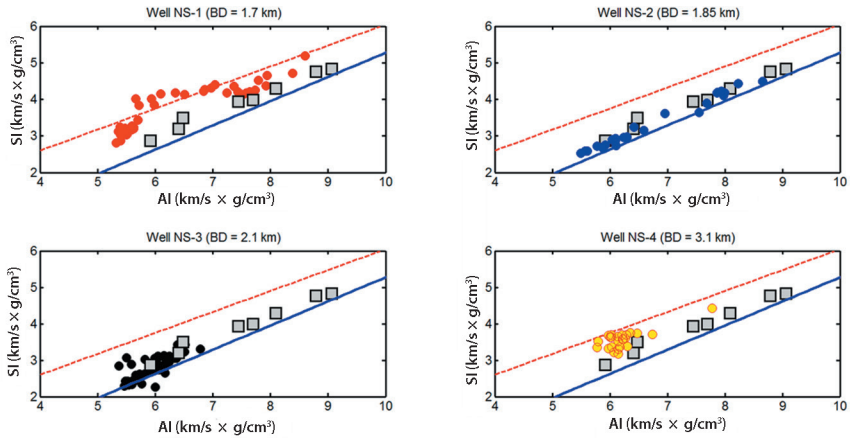

Figure 5. Crossplotting the Draupne Formation Shale in four North Sea wells, juxtaposed with the linear wet-shale trend (blue) and hot-shale trend (red). Gray squares are laboratory measurements of Kimmeridge shales by Vernik (1995).

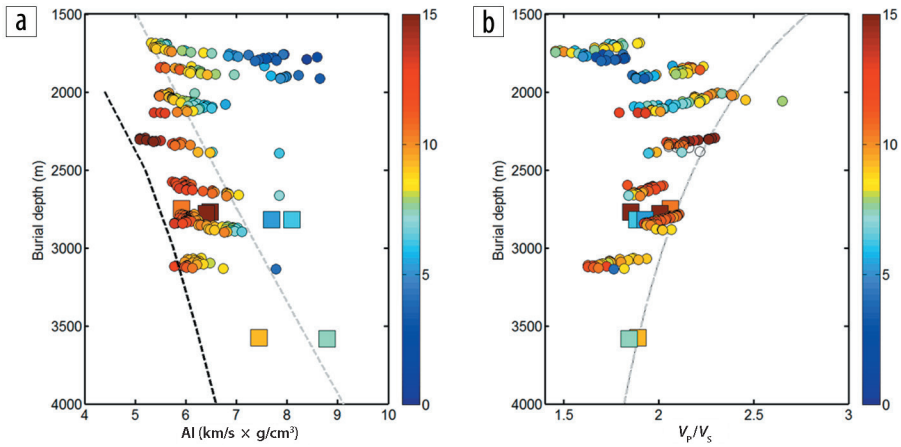

Figure 6. A compilation of well-log data from Kimmeridge Shale in selected wells from the North Sea and Norwegian Sea. Many competing effects result in quite a large scatter at a given burial depth, but still we see weak depth trends in both (a) acoustic impedance and (b) V_P/V_S . The data of Vernik (1995) are superimposed (large squares). The data are colored as a function of TOC content (wt%). Normal shale compaction trends (based on Storvoll et al., 2005) are superimposed (dashed gray lines), as well as a high TOC trend for AI versus depth (dashed black line), adapted from Løseth et al. (2011).

burial depth is about 2.1 km. Here also, most of the data plots closer to the wet-shale trend, except some data points that plot closer to the hot-shale curve. We will have a closer look at this well in the rock-physics template analysis below.

In well NS-4, the burial depth is about 3.1 km, and this well is located in a more basinal setting. This burial depth corresponds to temperatures at which we expect the oil-prone marine source rock of the North Sea to have entered the oil window (about 100°C to 120°C; see Glennie, 1998) because the temperature gradient in the North Sea is normally in the range of 35°C/km to 40°C/km. For this well, the Draupne Shale data plot closer to the hot-shale trend. What we see in this plot is likely the result of the fluid effect because the source rock has become mature.

In Figure 6, we plot the seismic properties of the Kimmeridge Shale intervals in selected wells from the Norwegian Sea and North Sea as a function of burial depth. The data are colored as a function of TOC content, estimated using equation 1. We also superimpose the ultrasonic measurements done by Vernik (1995) on Kimmeridge Shale, seen as large squares. We see that at a given burial depth, there is quite a large spread in acoustic impedance and V_P/V_S. This is likely because of variability in composition.

First of all, the TOC content varies significantly within the Kimmeridge Shale, and this affects both AI and V_P/V_S, in agreement with observations by Vernik and Liu (1997) and by Løseth et al. (2011). Another reason for the large scatter at a given depth is the fact that the Kimmeridge Shale can be quite calcareous and marly, particularly near structural highs (Bjørlykke, 2015). Calcite will tend to stiffen the rock frame, and acoustic impedance will increase drastically, whereas V_P/V_S will tend to drop slightly or remain the same. The increase in carbonate material will tend to dilute the organic content.

Hence, increase in acoustic impedance is caused by the combination of decreasing TOC and increasing carbonate material. This might explain the relatively large acoustic impedances and low V_P/V_S in the Kimmeridge shales in some of the shallowest wells included in Figure 6.

Furthermore, silica diagenesis associated with smectite-to-illite transformation and associated quartz cementation (Bjørlykke, 2015) might explain stiffening of the Kimmeridge Shale that will affect both AI and V_P/V_S. For deeper wells, where we expect Kimmeridge Shale to be mature, the generation and expulsion of hydrocarbons will affect the seismic properties also. We would expect the presence of gas and oil to result in decreasing acoustic impedance.

In spite of all the competing effects, we can see a weak depth trend in acoustic impedance and V_P/V_S in Figure 6; acoustic impedance increases slightly, whereas V_P/V_S decreases slightly. We have superimposed an empirical normal shale depth trend (V_P from Storvoll et al., 2005, combined with Gardner's equation to estimate density and the Greenberg-Castagna equation to estimate V_S; see Mavko et al., 2009). We see that the high end member of V_P/V_S data follows this trend nicely, whereas acoustic impedances show a much more gentle depth trend than the normal shale trend. We also have superimposed the high TOC bound in AI versus burial depth defined by Løseth et al. (2011) that nicely fits our most TOC-rich data.

The shallowest well-log data in Figure 6, representing well NS-1, shows the largest deviation in V_P/V_S from the background trend, with V_P/V_S values approaching 1.5 to 1.6. Those values cannot be explained by the presence of carbonate material alone

because the V_P/V_S ratio of calcite is about 1.9. The observed values are typical for gas-saturated sandstones. We will look at this in more detail in the rock-physics template analysis below.

Rock-physics templates

In this section, we do a more detailed rock-physics analysis of some of the selected wells above. We create rock-physics templates that honor the effect of maturation and conversion of kerogen to oil and gas. We use the approach introduced by Carcione et al. (2011) and further developed by Carcione and Avseth (2015). Here, we use rock-physics templates that show the transition from kerogen only to kerogen plus hydrocarbons or the transition from immature to mature source rocks. Pore-pressure effects can be included, but in this article, we assume that those effects have been released, and hydrostatic pressure is maintained.

Figure 7 shows well-log data from two neighboring wells, NS-2 and NS-3, including gamma ray, acoustic impedance, and V_P/V_S. The Draupne Formation shales are characterized by the very high gamma-ray values at about 200 API or higher. Note the sudden intra-Draupne increase in acoustic impedance and corresponding drop in V_P/V_S in well NS-2, not seen in NS-3.

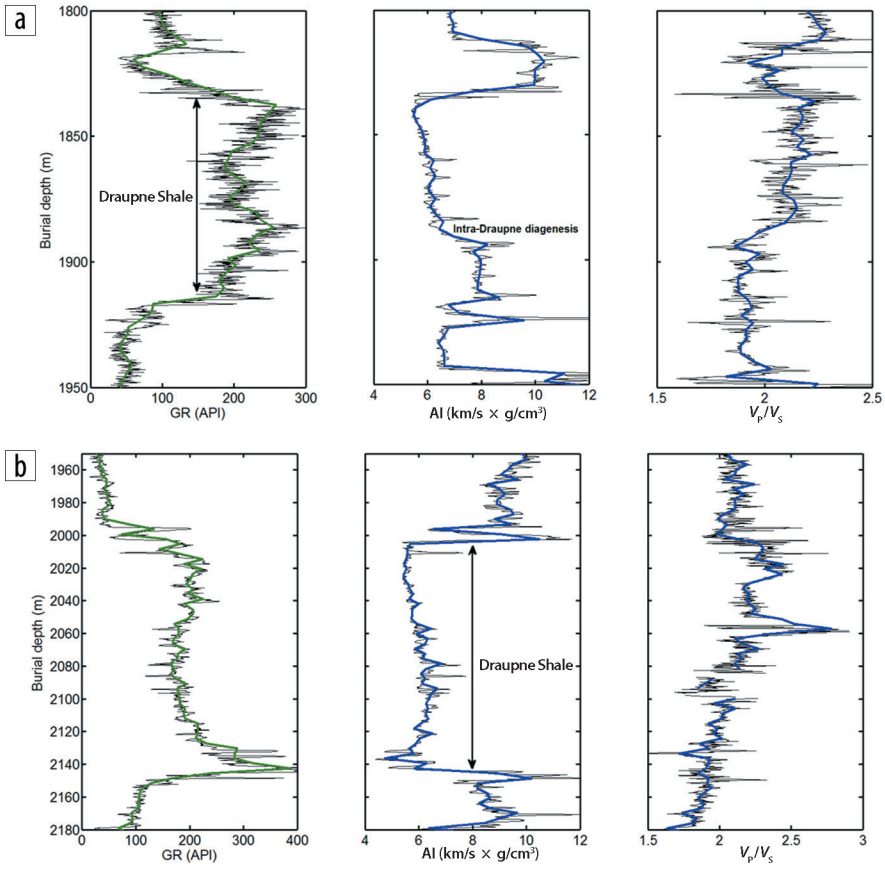

Figure 7. Well-log data from wells (a) NS-2 and (b) NS-3, including gamma ray, acoustic impedance, and V_P/V_S .

We crossplot both AI versus V_P/V_S and AI versus SI in Figure 8. Big black or gray circles represent upscaled well-log data, whereas smaller black or gray stars represent well-log data at the original scale. We superimpose the wet-shale and hot-shale reference curves and the rock-physics templates for mature organic-rich shale. We assume a shale porosity of 0.05 and volume of kerogen prior to hydrocarbon conversion of 0.2, that is, TOC of about 8% (representative for Kimmeridge Shale buried at about 2.5 to 3 km; see Carcione and Avseth, 2015).

We see that for well NS-2, the data split into two populations (gray circles and stars), one with relatively low AI and high V_P/V_S and one with higher AI and lower V_P/V_S. However, both populations fall near the wet-shale reference trend. This indicates that the changes seen in this well, with the sudden increase in AI and decrease in V_P/V_S, are likely to a diagenetic effect or consolidation caused by presence of carbonate material in the lower part of the Draupne Shale. None of the data falls inside the rock-physics template for the mature source rock, and we conclude that in this well, the Draupne Shale is still immature.

For the other well, NS-3, where the Draupne Shale is penetrated more downflank on the Horda Platform and therefore is buried more deeply, we see different trends (black circles and stars). Now we see a clear branch of the data plotting into the rock-physics template where we expect mature source rocks. The lowermost section of the well-log data plots with relatively low acoustic impedance and somewhat lower V_P/V_S than the rest of the interval, which falls closer to the wet-shale trend. What we see here could be the early maturation stage, when the lower part of the organic-rich shale in this well has started to generate hydrocarbons, and we would expect oil to be present.

Note that the rock-physics template predicts a slight increase in V_P/V_S with increasing oil saturation when gas saturation is zero, associated with the increase in kerogen porosity during oil generation. This is not clearly seen in the data. However, small amounts of associated gas might be generated even during early maturation stage, and as the template predicts, a small amount of gas will cause a significant decrease in V_P/V_S.

Next we compare the Draupne Formation in wells NS-1 and NS-2. These wells are only 6 km apart, and as mentioned above, the rock-physics properties showed different trends in these two wells. In fact, well NS-1 was drilled based on an AVO class III/soft ultrafar AVO anomaly within the Upper Jurassic interval, just downflank from the Troll field, as observed in the map in Figure 9. The predrill play model was eroded Jurassic sands from the structural highs redeposited as submarine sands farther downflank and later capped by Upper Jurassic organic-rich shales.

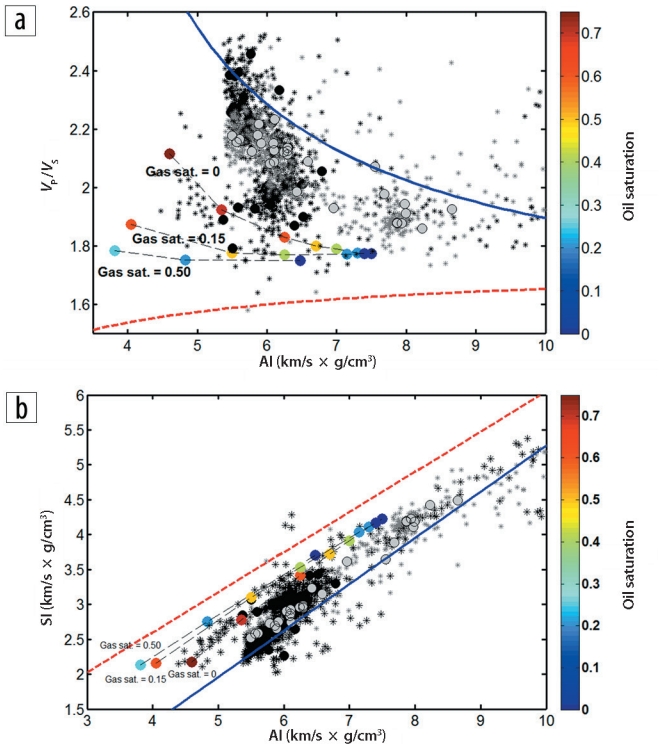

Figure 8. Crossplots of (a) AI versus V_P/V_S and (b) AI versus SI, including data from wells NS-2 (gray stars = well-log data; gray circles = upscaled well-log data) and NS-3 (black stars and circles). Rock-physics templates for mature source rocks with a mixture of kerogen, oil, and gas are superimposed. Most of the data plots along the wet-shale trend (blue line), but some data in well NS-3 plots closer to the hot-shale reference curve (dashed red line) and within the area of the rock-physics template. This possibly reflects early maturation at the base of the Draupne Formation in well NS-3.

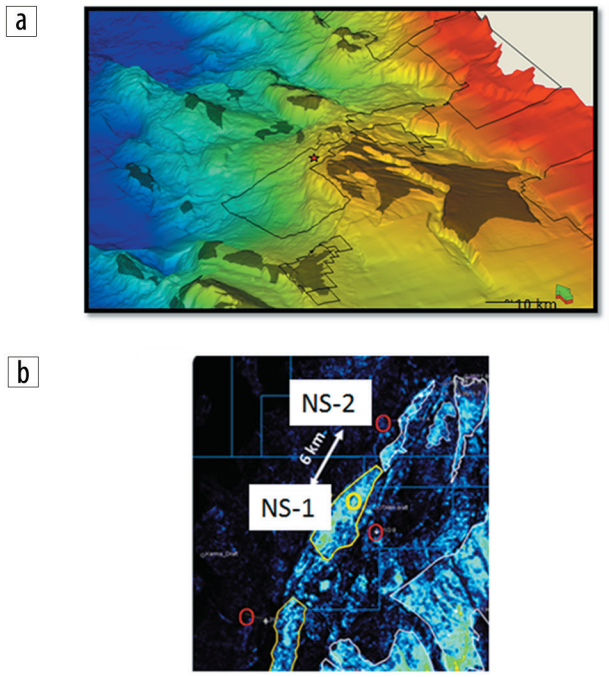

Figure 9. (a) Structural map and (b) AVO attribute map from the Horda Platform area. Bright colors (green, cyan) in the AVO attribute map indicate a soft ultrafar AVO anomaly in the Upper Jurassic interval. The tip of the Troll field can be seen to the southeast in the AVO map. Well NS-1 targeted an AVO anomaly downflank from Troll. NS-2 is 6 km north of NS-1 and had no AVO anomaly.

One of the pitfalls was a false-positive AVO anomaly caused by the organic-rich shale itself, but the calibration point at well NS-2 (drilled prior to NS-1) indicated that a thick Draupne Formation Shale would not give a class III AVO anomaly but a class IV, which is also in agreement with what is normally expected in organic-rich shales on the Norwegian Shelf (e.g., Løseth et al., 2011). The well, however, encountered only organic-rich shales in the target interval, and no sands.

Figure 10 shows well-log data from this well. The acoustic-impedance profile looks quite similar to what we observed in NS-2, with also a sharp increase in acoustic impedance within the Draupne Formation. However, we observe V_P/V_S ratios down to 1.5 to 1.6 within the Draupne Shale, which we did not observe in well NS-2.

In Figure 11, we crossplot the Draupne Shale data in wells NS-1 and NS-2 together. Here we see the dramatic difference between these two wells. The impedance values show similar ranges, but the V_P/V_S ratios in NS-1 are significantly lower than in NS-2. The Draupne Shale in NS-1 plots as a "banana" shape between the wet-shale trend and the hot-shale trend. In fact, many of the data points fall right on top of the hot-shale trend.

However, the data do not comply with the rock-physics template for mature source rocks. The geochemical studies and headspace gas-chromatography analysis conducted for well NS-1 confirmed the presence of low gas saturation (both methane and CO_2), up to 10%, at the depth level where the V_P/V_S values are at their lowest (1.5 to 1.6). However, basin modeling has indicated that the source rock is likely to be immature at this burial depth, which is also manifested by relatively high hydrogen-index values, mostly 450 to 500. The confirmed presence of low-saturation gas (both methane and CO_2) might be related to early generation from hyperreactive kerogen types or migrated gas generated nearby at deeper burial. The presence of low gas saturation explains the anomalously low V_P/V_S ratios in this well.

The combination of carbonate material, diagenesis, and possibly fractures within this rock can be why the rock-physics template for mature source rock does not explain the data well because the template does not take into account the presence of carbonates or fractures.

Discussion

Rock-physics analysis of the Kimmeridge Shale equivalent in selected wells in the Norwegian Sea and North Sea indicate some interesting but complex trends. The combined effects of organic richness, mineral composition, diagenesis, and maturation give large scatters in rock-physics crossplots. The complexity of these rocks and the lack of geochemical and geophysical information in many wells make it challenging to predict the quality of the source rocks from seismic prior to drilling. However, based on the limited well-log data available in this study, along with information from the

rock-physics template models, there seem to be a few rules of thumb that we can benefit from during hydrocarbon exploration and seismic source-rock characterization.

First of all, the presence of TOC seems to cause a strong decrease in acoustic impedance, as shown in Figure 6 (c.f. Vernik and Liu, 1997, and Løseth et al., 2011). Compaction and diagenesis will cause an increase in impedance. The effect of TOC on V_P/V_S is more ambiguous, as we also observe in Figure 6. For some of the wells, V_P/V_S seems to increase with TOC, whereas for other wells, we see the opposite trend. The inconsistent pattern is likely a result of the many competing factors that affect V_P/V_S ratios. For instance, it could be difficult to disentangle the effect of maturation (i.e., hydrocarbon generation and expulsion) and organic richness.

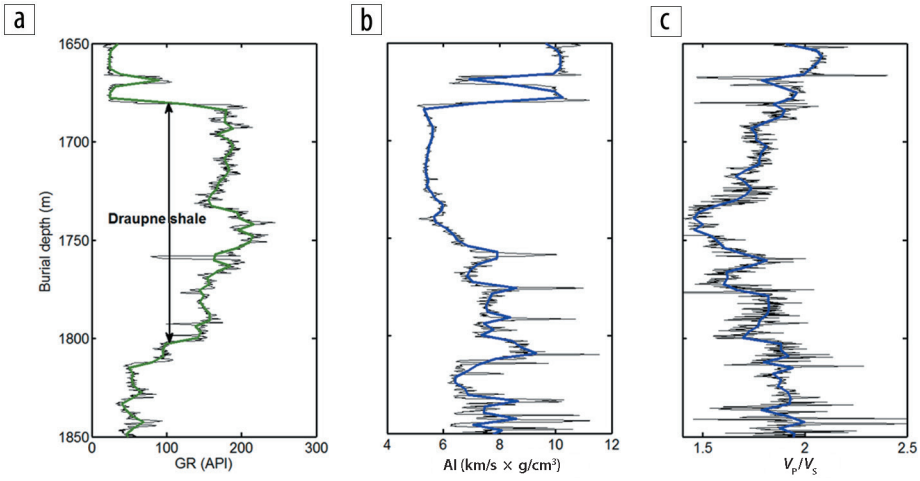

Figure 10. Well-log data in well NS-1, including (a) gamma ray, (b) acoustic impedance (AI), and (c) V_P/V_S . Black curves are well-log data in original scale; blue curves are upscaled curves. Note the very low V_P/V_S ratios (1.5 to 1.6) in the Draupne Formation Shale in this well.

However, some studies (e.g., Qin et al., 2014) have indicated that TOC will cause a drop in V_P/V_S independent of thermal maturity. Qin et al. (2014) also show that the separate effect of maturation would cause a decrease in V_P/V_S and that the combined effect of TOC and maturation could explain the very low V_P/V_S observed in mature, organic-rich Bakken Formation shales.

For the Norwegian Shelf organic-rich shales, these effects likely are counteracted by the high clay content typical of the Kimmeridge Shale. Hence, the V_P/V_S decrease is normally more subtle than what is observed in more marly source rocks. Moreover, a carbonate-rich section of Kimmeridge with relatively low TOC can have lower V_P/V_S than a clay-rich section of Kimmeridge with relatively high TOC. Relative to a wet-shale (i.e., inorganic) trend, however, we find that both organic richness and presence of hydrocarbons will shift the Kimmeridge Shale data points toward the hot-shale trend, i.e., lower V_P/V_S ratio.

In well NS-4, the Draupne Shale is located at burial depths where temperatures are within the oil window (about 110°C to 120°C). This is the well where the Kimmeridge data plot closest to the hot-shale trend, except the data in well NS-1 (Figure 5). However, in the latter well, headspace gas chromatography confirmed presence of low gas saturation corresponding with the zone of very low V_P/V_S ratios. Because well 6507/11-6 in the Norwegian Sea, with higher TOC than in well NS-1, plotted with higher V_P/V_S, we interpret the low V_P/V_S in well NS-1 to be caused by the presence of gas.

The rock-physics templates used in this study take into account smectite-to-illite transition, porosity compaction with depth, and kerogen conversion to oil and associated gas. These templates seem to describe some of the data in this study but might not work for all organic-rich shales, particularly where carbonate matter is present or more complex diagenetic processes have taken place. In addition, we have not included the

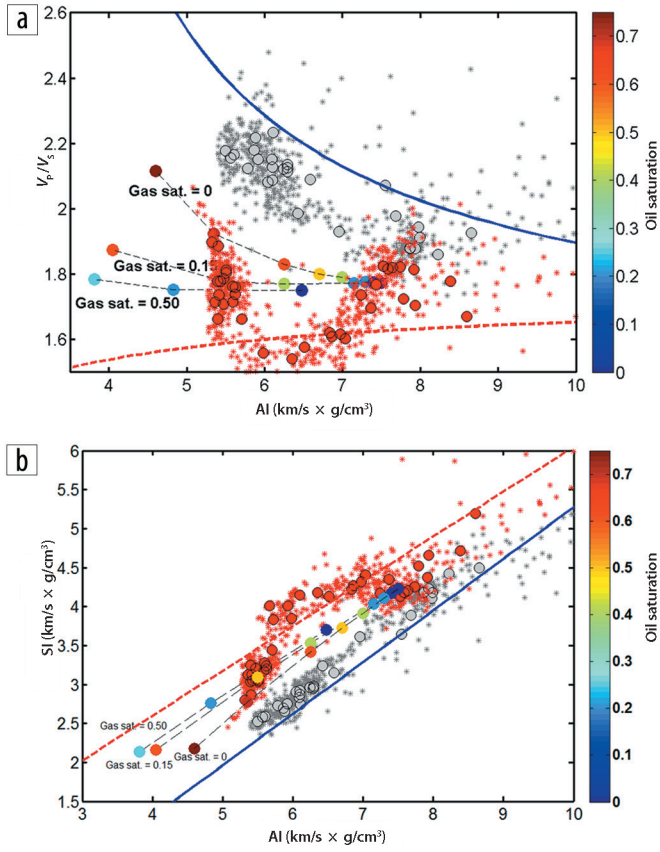

Figure 11. Crossplot of (a) AI versus V_P/V_S and (a) AI versus SI for the Draupne Shale in wells NS-1 (red stars and circles) and NS-2 (gray stars and circles). Note how the Draupne Shale in NS-1 deviates strongly from the trend seen in well NS-2. The data plot more closely to the hot-shale reference trend (dashed red curve). Headspace gas chromatography confirmed the presence of low gas saturation in NS-1, even though the Draupne Shale is found to be immature in this well. The superimposed rock-physics template for mature source rock does not fit very closely with the data in either well.

effect of overpressure in this study, but Carcione and Avseth (2015) show how this can be included in the templates.

Several authors have reported on the complex fluid-saturation patterns that can occur in organic-rich shales at different maturation stages (e.g., Passey et al., 2010; Sondergeld et al., 2013), with gas located in micropores and oil filling larger cracklike porosity. In this study, we have modeled only hydrocarbons within the kerogen phase, and with only one type of porosity. Future research should focus on how we can improve our models to be even more geologically and physically realistic. At the same time, it is important to not overparameterize the problem in an explorational setting where it is challenging to calibrate our rock-physics models.

Conclusions

We have investigated rock-physics trends and properties of clay-rich source rocks in selected wells in the North Sea and Norwegian Sea. We find that nearly all the source-rock data in the study are bounded nicely by linear trends that are based on rock-physics models, in acoustic-impedance versus shear-impedance crossplots. These reference models serve as a nice screening tool for organic richness and/or maturation level (i.e., hydrocarbon generation and expulsion), regardless of burial depth. We also demonstrated the use of rock-physics templates for the early mature to mature stage of clay-rich source rocks by combining a simple basin-modeling approach with a rock-physics model using the Backus average in which the organic-rich shale is represented by a transverse isotropic mixture of clays, kerogen, and hydrocarbons. The resulting templates are bounded nicely by the Vernik reference trends and explain some of the observed trends in the data. However, the local presence of carbonaceous material and diagenesis within the source rock, which have not been accounted for in the rock-physics modeling, might explain why some of the data points have higher impedances and lower V_P/V_S than the template models. Finally, we have shown that source rocks with hydrocarbon saturation can cause AVO signatures similar to hydrocarbon-filled sands and therefore represent false positives in exploration. TLE

Acknowledgments

Thanks to Tullow Oil Norge for allowing us to publish this study. Thanks to partners of license PL550 (VNG and Det Norske) for allowing us to publish data from the license. Also thanks to Richard Olstad, Tullow Oil, and Tor Veggeland, formerly at Tullow Oil, for valuable input to this work. Finally, thanks to Lev Vernik at Seismic Petrophysics LLC for valuable comments.

Corresponding author: Per.Avseth@tullowoil.com

References

Avseth, P., T. Veggeland, and F. Horn, 2014, Seismic screening for hydrocarbon prospects using rock-physics attributes: The Leading Edge, **33**, no. 3, 266–274, http://dx.doi.org/10.1190/tle33030266.1.

Bandyopadhyay, K., R. Sain, E. Liu, C. Harris, A. Martinez, and M. Payne, 2012, Rock property inversion in organic-rich shale: Uncertainties, ambiguities and pitfalls: 82nd Annual International Meeting, SEG, Expanded Abstracts, http://dx.doi.org/10.1190/segam2012-0932.1.

Bjørlykke, K., ed., 2015, Petroleum geoscience — From sedimentary basins to rock physics, 2nd ed.: Springer Verlag.

Carcione, J. M., and P. Avseth, 2015, Rock-physics templates of clay-rich source rocks: Geophysics, **80**, no. 5, D481–D500, http://dx.doi.org/10.1190/geo2014-0510.1.

Carcione, J. M., H. B. Helle, and P. Avseth, 2011, Source-rock seismic-velocity models: Gassmann versus Backus: Geophysics, **76**, no. 5, N37–N45, http://dx.doi.org/10.1190/geo2010-0258.1.

Glennie, K. W., ed., 1998, Petroleum geology of the North Sea — Basic concepts and recent advances, 4th ed.: John Wiley & Sons, http://dx.doi.org/10.1002/9781444313413.

Hu, R., L. Vernik, L. Nayvelt, and A. Dicman, 2015, Seismic inversion for organic richness and fracture gradient in unconventional reservoirs: Eagle Ford Shale, Texas: The Leading Edge, **34**, no. 1, 80–84, http://dx.doi.org/10.1190/tle34010080.1.

Khadeeva, Y., and L. Vernik, 2014, Rock-physics model for unconventional shales: The Leading Edge, **33**, no. 3, 318–322, http://dx.doi.org/10.1190/tle33030318.1.131350

Løseth, H., L. Wensaas, M. Gading, K. Duffaut, and M. Springer, 2011, Can hydrocarbon source rocks be identified on seismic data?: Geology, **39**, no. 12, 1167–1170, http://dx.doi.org/10.1130/G32328.1.

Mavko, G., T. Mukerji, and J. Dvorkin, 2009, The rock physics handbook: Tools for seismic analysis of porous media, 2nd ed.: Cambridge University Press, http://dx.doi.org/10.1017/CBO9780511626753.

Passey, Q. R., K. M. Bohacs, W. L. Esch, R. Klimentidis, and S. Sinba, 2010, From oil-prone source rock to gas-producing shale reservoir — Geologic and petrophysical characterization of unconventional shale gas reservoirs: CPS/SPE International Oil and Gas Conference and Exhibition in China, SPE conference paper 131350-MS, http://dx.doi.org/10.2118/131350-MS.

Qin, X., D.-H. Han, and L. Zhao, 2014, Rock physics modeling of organic-rich shales with different maturity levels: 84th Annual International Meeting, SEG, Expanded Abstracts, 2952–2957, http://dx.doi.org/10.1190/segam2014-1584.1.

Sondergeld, C. H., C. S. Rai, and M. E. Curtis, 2013, Relationship between organic shale microstructure and hydrocarbon generation: SPE Unconventional Resources Conference, USA, SPE conference paper 164540-MS, http://dx.doi.org/10.2118/164540-MS.

Storvoll, V., K. Bjørlykke, and N. Mondol, 2005, Velocity-depth trends in Mesozoic and Cenozoic sediments from the Norwegian Shelf: AAPG Bulletin, **89**, no. 3, 359–381, http://dx.doi.org/10.1306/10150404033.

Tissot, B. P., and D. H. Welte, 1984, Petroleum formation and occurrence: Springer Verlag, http://dx.doi.org/10.1007/978-3-642-87813-8.

Vernik, L., 1995, Petrophysics of the Kimmeridge Shale, North Sea: Stanford Rock Physics Laboratory.

Vernik, L., and M. Kachanov, 2010, Modeling elastic properties of siliciclastic rocks: Geophysics, **75**, no. 6, E171–E182, http://dx.doi.org/10.1190/1.3494031.

Vernik, L., and C. Landis, 1996, Elastic anisotropy of source rocks: Implications for hydrocarbon generation and primary migration: AAPG Bulletin, **80**, no. 4, 531–544.

Vernik, L., and X. Liu, 1997, Velocity anisotropy in shales: A petrophysical study: Geophysics, **62**, no. 2, 521–532, http://dx.doi.org/10.1190/1.1444162.

Vernik, L., and J. Milovac, 2011, Rock physics of organic rich shales: The Leading Edge, **30**, no. 3, 318–323, http://dx.doi.org/10.1190/1.3567263.